Use of local electrochemical methods (SECM, EC-STM) and AFM to differentiate microstructural effects (EBSD) on very pure copper

Martinez Lombardia, Esther; Lapeire, Linsey; Maurice, Vincent; De Graeve, Iris; Klein, Lorena; Marcus, Philippe; Verbeken, Kim; Kestens, L.A.I.; Gonzalez Garcia, Yaiza; Mol, Arjan

DOI
10.14773/cst.2017.16.1.1

Publication date
2017

Document Version
Final published version

Published in
Corrosion Science and Technology

CORROSION SCIENCE AND TECHNOLOGY, Vol.16, No.1(2017), pp.1~7
[Research Paper]
pISSN: 1598-6462 / eISSN: 2288-6524
DOI: https://doi.org/10.14773/cst.2017.16.1.1

Use of Local Electrochemical Methods (SECM, EC-STM) and AFM to Differentiate Microstructural Effects (EBSD) on Very Pure Copper

Esther Martinez-Lombardia[1], Linsey Lapeire[2], Vincent Maurice[3], Iris De Graeve[1], Lorena Klein[3], Philippe Marcus[3], Kim Verbeken[2], Leo Kestens[2,4], Yaiza Gonzalez-Garcia[4], Arjan Mol[4], and Herman Terryn[1,4,†]

[1]*Vrije Universiteit Brussel, Research Group Electrochemical and Surface Engineering, Pleinlaan 2 B-1050 Brussels, Belgium*
[2]*Ghent University, Department of Materials Science and Engineering, Technologiepark 903 B-9052 Zwijnaarde (Ghent), Belgium*
[3]*CNRS - Chimie ParisTech (UMR 8247), Institut de Recherche de Chimie Paris, 11 rue Pierre et Marie Curie, F-75005 Paris, France*
[4]*Delft University of Technology,Department of Materials Science and Engineering, Mekelweg 22628 CD Delft,The Netherlands*

(Received September 21, 2016; Revised September 21, 2017; Accepted January 04, 2017)

When aiming for an increased and more sustainable use of metals a thorough knowledge of the corrosion phenomenon as function of the local metal microstructure is of crucial importance. In this work, we summarize the information presented in our previous publications[1-3] and present an overview of the different local (electrochemical) techniques that have been proven to be effective in studying the relation between different microstructural variables and their different electrochemical behavior. Atomic force microscopy (AFM)[1], scanning electrochemical microscopy (SECM)[2], and electrochemical scanning tunneling microscopy (EC-STM)[3] were used in combination with electron backscatter diffraction (EBSD). Consequently, correlations could be identified between the grain orientation and grain boundary characteristics, on the one hand, and the electrochemical behavior on the other hand. The grain orientation itself has an influence on the corrosion, and the orientation of the neighboring grains also seems to play a decisive role in the dissolution rate. With respect to intergranular corrosion, only coherent twin boundaries seem to be resistant.

Keywords: *copper, microstructure, EBSD, EC-STM, AFM, SECM*

1. Introduction

In order to increase the sustainability of metals, a more detailed understanding of the corrosion process is of crucial importance. Till now corrosion was often consider as a purely chemical interaction with an exclusive dependence on compositional effects, while ignoring microstructural and crystallographic properties of the metal surface [4-11]. Some recent literature data, however, suggest an important effect of microstructural elements such as grain size, crystallographic orientation and grain boundary characteristics features on the electrochemical behavior [12-22].

Thermomechanical processing can be used to change to a certain extent the microstructure of different metals; change their texture or to control the length fraction and type of grain boundaries. This microstructural changes could potentially enhance and increase the durability of the materials. However, before these "engineered materials" can be developed, it is necessary to fully understand the local electrochemical behavior and how this is related with the different microstructural parameters.

The aim of this work is to obtain a better understanding of the relation between the corrosion behavior of a metal and its microstructural variables. The grain dependent electrochemical behavior of polycrystalline copper was confirmed by using several local electrochemical techniques. The results presented in this work summarize the influence of the crystallographic orientation on the active dissolution of copper observed with different individual methods [1-3]. The overall conclusions are drawn from both ex situ Atomic force microscopy (AFM) measurements and in situ Scanning electrochemical microscopy (SECM) experiments in combination with EBSD imaging. Electrochemical Scanning tunneling microscope (EC-STM) was used to visualize the differences in intergranular corrosion at different grain boundaries.

2. Experimental

2.1 AFM experiments

Cast ETP-Cu was obtained from Aurubis® (Belgium).

† Corresponding author: hterryn@vub.ac.be

The first step is to apply a hot rolling at 350 °C (75% thickness reduction) in order to change the as-cast microstructure to a completely new recrystallized one. For the AFM measurements, a subsequent cold rolling was applied (80% thickness reduction) followed by an annealing treatment of 60 min at 250 °C. Subsequently, the material was mechanically ground and polished, finishing with 1 µm diamond paste. The sample was then immersed during 210 min in 0.1 M NaCl. Subsequently, AFM topography measurements were performed using a Veeco CP II system. To obtain a suitable surface preparation for EBSD, a final electropolishing step (10 V, 10 s) in a phosphoric acid electrolyte was necessary.

2.2 SECM experiments

For the SECM experiments a bigger grain size adapted to the lateral resolution of the system was necessary. The hot rolling samples were annealed for 24 h at 800 °C. Subsequently, the material was grinded and polished, finishing with 1 µm diamond paste. Prior to the SECM measurements, the texture of the polycrystalline copper samples was characterized by EBSD. A final electropolishing step (10 V during 10 s) in a phosphoric acid electrolyte was necessary.

The selected working mode was feedback mode, using ferrocenemethanol as an electrochemical mediator. Operating in this mode it is possible to distinguish different electrochemical reactivity of the surface. The oxidation of Fe(II) to Fe(III) from the electrochemical mediator is the selected reaction at the micro electrode. The tip current at the proximities of the metal surface is a function of the nature of the substrate, making it possible to distinguish more or less active areas (grains). In the case of a not active grain, the current at the tip will be lower than the limiting current measured at the bulk of the solution (negative feedback). This in contrast to the proximities of an electroactive surface (grain being actively corroded), for which the current at the tip will increase, since the substrate is able to regenerate Fe(II) from the reduction of Fe(III) formed at the microelectrode and hence induces a redox cycling leading to a positive feedback. Two different experiments were performed: Copper in active dissolution state, and passivated copper. A 10µm tip electrode was used in both cases. The size of the SECM microelectrode, the mapping rate and dimensions were carefully selected to reach a good compromise between adequate spatial resolution and sufficiently fast scans to monitor the reactivity of copper during its fast dissolution.

SECM measurements of copper in active state were performed in 5 mM NaCl solution containing ferrocenemethanol as the electrochemical mediator. The sample was maintained at OCP.

For the SECM measurements in the passive state the sample was used as a secondary working electrode, this was necessary in order to do the electrochemical characterization and passivation of the sample. The passivation of the sample was performed in 0.1 M NaOH solution. Before forming the passive layer, the native oxide layer was reduced by scanning the potential in the cathodic direction till -1.5 V vs Ag/AgCl. The sample was then passivated by polarizing during 30 min at +0.1 V vs Ag/AgCl. After passivation, the electrolyte was removed and the cell was thoroughly cleaned with bidistilled water. After cleaning, the cell was filled with a sodium hydrogen orthophosphate/sodium hydroxide buffer solution (pH=12) containing 5 mM ferrocenemethanol as a mediator and experiments on the feedback mode were performed.

2.3 ECSTM experiments

For the study with ECSTM, a suiFig. grain size for the STM field of view was of great importance. Cryogenic

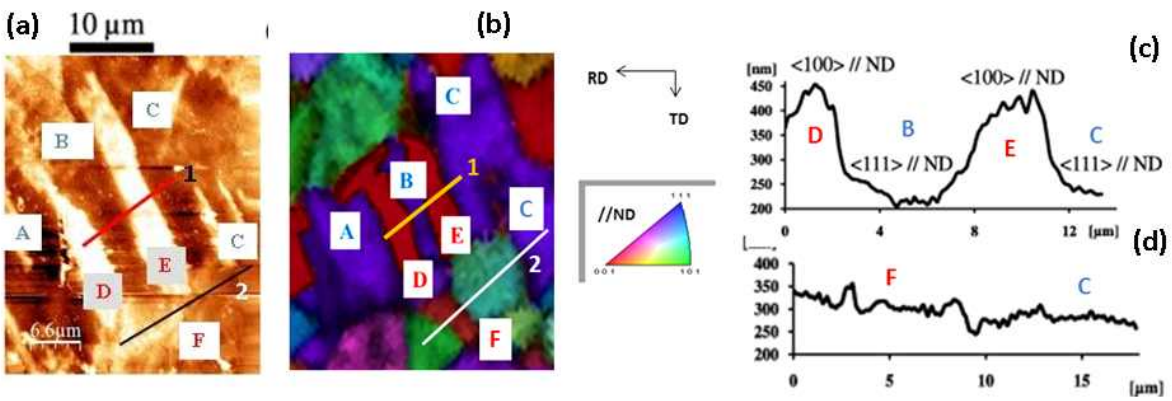

Fig. 1 Topographic map measured by AFM with indication of two line scans (a) and combined inverse pole figure (IPF)/image quality (IQ) map (b) of the Cu sample. Line scan of the line indicated in red (c) and black (d) on the topographic map [1].

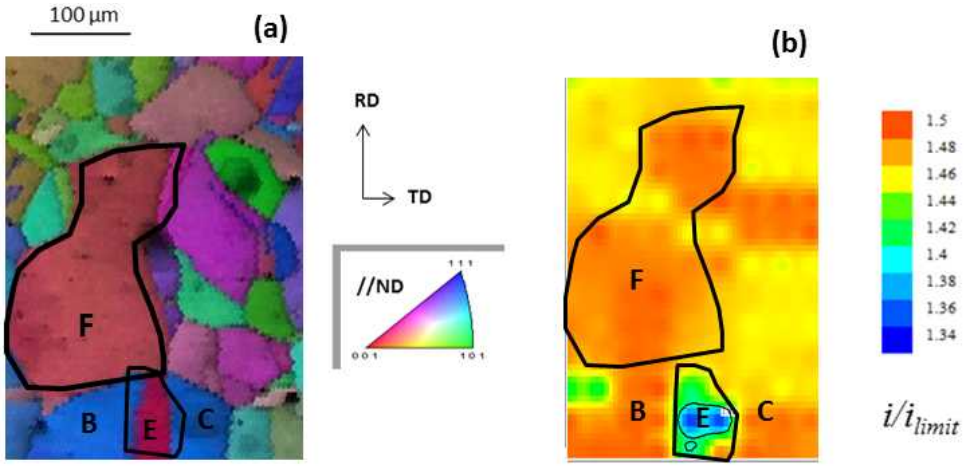

Fig. 2 Combined inverse pole figure (IPF)/image quality (IQ)map (a) and corresponding SECM current map (b). Scanned area 400µm in x and y direction with dx=10µm and dy=20µm, experiments in the active dissolution state. Area involving <111>// ND (B and C) and <001>// ND (E and F) oriented grains [2].

deformation, previously proposed to produce microcrystalline or nanocrystalline materials [23,24], was used. The samples were prepared by cryogenic rolling after cooling the sample with liquid nitrogen. The final reduction of the sample thickness was 91%. After this mechanical treatment, the samples were annealed for 1 min at 200 °C. These parameters were carefully selected in order to ensure full recrystallization of the grains while maintaining a suitable grain size for the field of view of the ECSTM scanner (10 µm × 10 µm). The surface was prepared by mechanical polishing with diamond paste down to 0.25 µm grade followed by electrochemical polishing in 60% orthophosphoric acid during 4 min at 1.4 V versus a copper electrode.

2.4 EBSD

The EBSD system is attached to a Field emission scanning electron microscope (FE-SEM) operated at 20 kV. Measurements were carried out with a step size selected according to the grain size of the different samples. The orientation data were post-processed with the commercial orientation imaging software package OIM- TSL®. The orientation images are represented as inverse pole figure (IPF) maps, i.e. the color of each grain represents the crystal orientation that is parallel to the sample surface normal (ND).

3. Resutls and Discussion

With the Atomic force microscopy (AFM) in combination with Electron backscatter diffraction (EBSD) relation between grain orientation and dissolution rate were observed [1]. The surface topography of the copper samples was visualized with AFM after exposure to different electrolytes; this allowed evaluating height differences between differently oriented grains. The corresponding crystallographic orientation data were obtained by EBSD. A large height difference is observed on the topographic map when adjacent grains have near <111> // ND (grains A, B and C) and <001> // ND orientation (grains D and E), with the <111> // ND orientations showing a higher dissolution rate. This is nicely illustrated with the line scan across grains D, B, E and C (Fig. 1c) which clearly shows the distinct dissolution rates between the differently oriented grains. The height profile along line 2, Fig. 1d, doesn't show significant differences between the grains. In this case both grains F and C with orientations close to <111> // ND and <001> // ND show similar surface levels, also similar to the surrounding grains. In this case <111> // ND and <001> // ND don't appear next to each other in the microstructure. If we compare the height levels for both <001>//ND grains E and F, E shows a mean height value around 420 nm and F around 300 nm confirming that the surrounding grains can play a decisive role on the corrosion rates.

This observation was further confirmed by means of SECM working in feedback mode [2]. Fig. 2, shows the combined inverse pole figure (IPF)/image quality (IQ) map and corresponding SECM normalized current map. Fig. 2b observes that current values in the whole area are higher than the limiting current (which is 1 for normalized current). This indicates that the surface of copper is electrochemically active which is expected since copper is easily corroded in NaCl. In Fig. 2b a higher current at the tip is measured above the grains B and C which

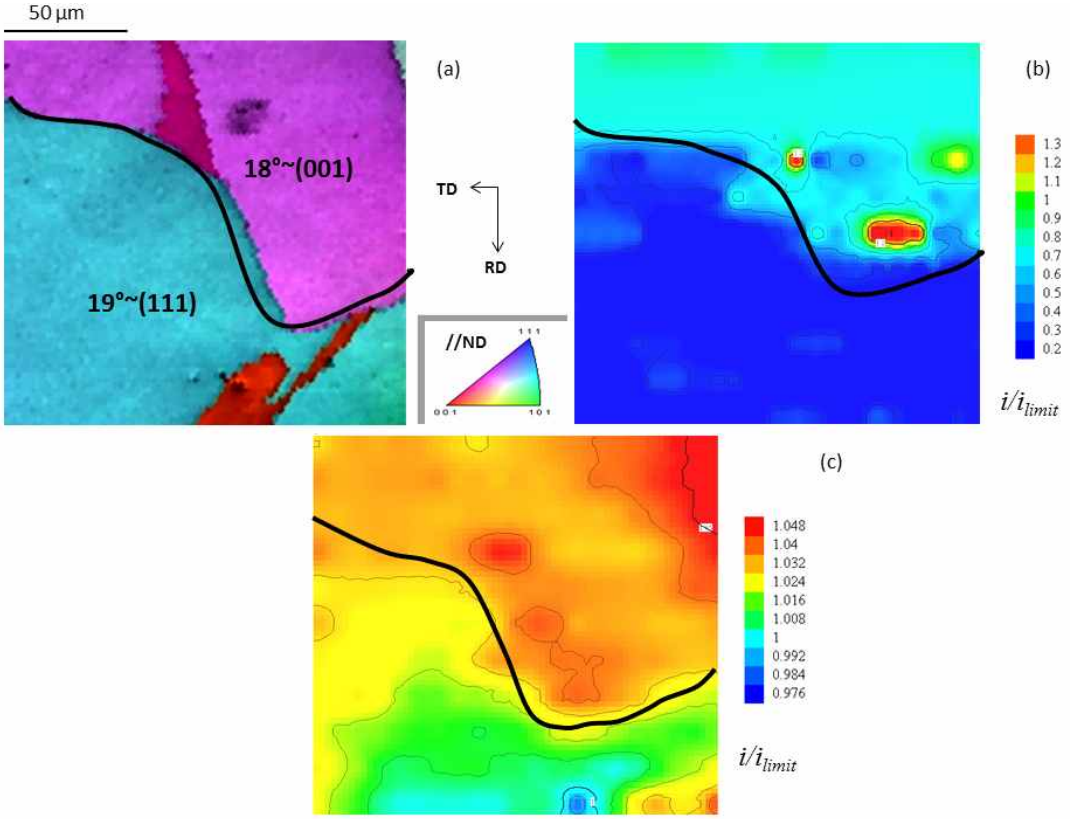

Fig. 3 Combined inverse pole figure (IPF)/image quality (IQ) map (a) and corresponding SECM current map after passivation at E = 0,1 V during 30min (b) corresponding SECM current map after the cathodic reduction of the passive layer (c). Measurements in sodium hydrogen orthophosphate/sodium hydroxide buffer solution containing 5mM ferrocenemethanol. Scanned area 200 µm in x and y direction with dx=10 µm and dy=20 µm [2].

are <111> // ND oriented grains, these grains have a neighboring grain which is nearly <001> // ND oriented, the grain configuration in this case is very similar to the one observed along line 1 in Fig. 1. It is also interesting to notice that grains F and E are both <001> // ND oriented grains, but the measured current is lower for the grain E which is completely surrounded by <111> // ND oriented grains. On the other hand the grain marked as F shows a higher current and in this case it is predominantly surrounded by grains with different orientations than <111> // ND.

This behavior can be described as if depending on the surrounding grains a grain may partially change its electrochemical behavior. As an example, if we have two grains interconnected on the copper surface, the partial anodic exchange current will be given by the grain with the "lower electrode potential" or more "anodic grain", while the partial cathodic exchange current will be given by the "more noble grain", or the grain with the "higher electrode potential". If on a different area, the exact same ‘’anodic grain" is now surrounded by "highly anodic grains" it is possible that the nature of this grain will partially change to act as the "cathode".

The lower current observed at grain E in Fig. 2.b could be a consequence of the "more anodic" surrounding grains <111> // ND, which are dissolving preferentially. In a way this could be seen as a similarity with the cathodic protection of metals; i.e if two metals are connected, the metal with the more negative electrode potential (anode) will corrode preferentially, protecting the other metal from corrosion. In this example, the grains B and C (<111> // ND) could be seen as the anode, being the grain E (<001> // ND) under cathodic protection.

Heterogeneities of the passive layer formed on adjacent grains with near <001> // ND and <111> // ND were also observed by means of SECM measurements [2].

Fig.3b shows selected SECM maps after formation of a passive oxide and corresponding EBSD image Fig. 3a. The SECM map after the passivation treatment shows currents under the limiting current value, which is expected for a passive surface. Furthermore a correlation between grain distribution and measured reactivity on the SECM

map by comparing Fig. 3a and Fig. 3b can be observed. The grain with an orientation closer to <111> // ND (tilted 19° from the elementary index planes) shows a lower current compared to the grain which orientation is closer to <001> // ND (tilted 18° from the elementary index planes), which confirms that grain orientation has an influence on the electrochemical reactivity of the passive layer generated on top. Passive layer with underlying <111> // ND oriented grain presented a higher insulating or non-active behavior than the layer formed on <001> // ND oriented grain.

In order to verify that the measured currents in Fig. 3b are related to the passive layer, an additional experiment was carried out. The sample was cathodically polarized till -1.4 V to force the reduction of the previously formed passive layer. Then a new SECM map on the same area was measured, showing normalized currents that are slightly higher than the limiting currents confirming that the non-active layer was partially reduced making the copper surface active again (see Fig. 3c). Even though the tip current differences between the two grains are not as great as when covered with the passive layer, a difference in current can still be seen, and the current above the <111> // ND oriented grain is lower, suggesting that the passive layer that was covering this grain was less easily reduced than the passive layer formed on the <001> // ND oriented grain.

It has been reported that the anodic oxide film on copper has a p-type [25,26] semiconductor behavior, where the electrons migrate to the surface from where they can react with an unoccupied (acceptor) state in the electrolyte, e.g. the oxidized form of ferrocenemethanol in our case. The electron-transfer between the electrochemically passivated surface and outer redox intermediates is considered to happen through an electron-tunneling controlled process [27]. The differences in the measured current are consequently due to a difference in the direct tunneling of the electrons through the oxide. This difference can be due to a thicker

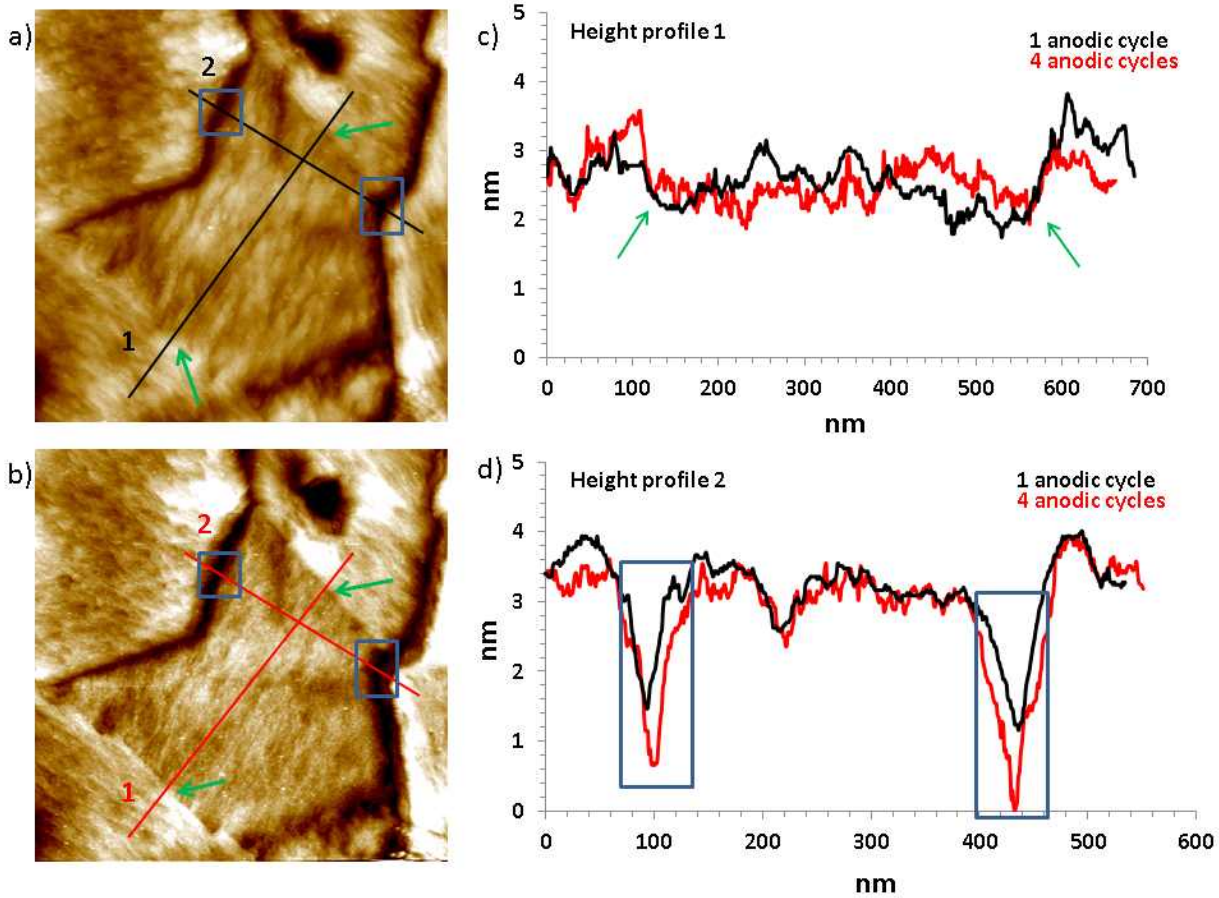

Fig. 4 Topographic ECSTM images of metallic surface of polycrystalline copper after (a) 1 and (b) 4 anodic cycles (X = Y = 700 nm, ΔZ = 4 nm, ECu= -0.05 V, Etip = -0.35 V, Itip = 2 nA) and height profiles along (c) line 1: Green arrows mark coherent twin grain boundaries and (d) line 2: blue rectangles mark random grain boundaries [3].

passive layer formed on the <111> // ND oriented grain or due to differences of the crystallinity or defect density of the passive layer that were previously reported [28]. It is well known that the grain boundary type has a big influence on the intergranular corrosion behaviour of a polycrystalline material [29]. A special boundary is one that has better corrosion properties compared to a random boundary. These special boundaries are known as coincident site lattice boundaries (CSLs) and are represented by Σ. Some authors claim that apart from Σ3 boundaries, the properties of CSLs in polycrystals are not different from those of random grain boundaries [30]. Moreover, it was demonstrated that Σ3 boundaries do not necessarily have good corrosion resistance properties. In 304 stainless steel, only coherent twin boundaries, Σ3 boundaries with a (111) grain boundary plane, were found to be resistant to intergranular corrosion [31].

In situ EC-STM was used to visualize the susceptibility to intergranular corrosion of different types of grain boundaries of a microcrystalline copper in HCl [3]. Anodic potentiodynamic polarization were performed in order to induce dissolution of the copper metal and to produce intergranular corrosion, the surface evolution was followed and compared after several anodic cycles.

Fig. 4 shows the sample topography after one (Fig. 4a) and four (Fig. 4b) anodic scans. Two straight grain boundaries (marked by green arrows) can be seen together With several curved grain boundaries. The evolution of the different grain boundaries is followed by cross section analysis. A considerable attack is observed for the curved grain boundary (height profile 2, Fig. 4d). The magnitude of intergranular corrosion is determined by both the penetration at the grain boundary and the dissolution at the surface of the grains that form the grain boundary. In this case, a significant depth penetration is measured. Fig. 4.c shows a height profile across the two straight grain boundaries. There is no indication of intergranular corrosion, since both profiles (obtained before and after anodic dissolution) are similar.

It was already discussed by several authors that when parallel sided grain boundaries appear on a microstructure, like the grains boundaries marked by green arrows in Fig. 4, these grain boundaries are most likely coherent twins [32]. In order to confirm this assumption, an area of 5050 mm^2 was studied by EBSD to determine the different morphologies of the grain boundaries. Among 227 grain boundaries, only one straight grain boundary was found to be a random high angle boundary. All other straight boundaries were found to be Σ3. On the other hand, when looking at the Σ3 boundaries, it was found that around 50% of them are straight and 50% are curved. It can be then concluded that a straight grain boundary has a very high probability to be a coherent twin boundary and that a curved grain boundary can be cataloged either as random high angle boundary or non coherent twin boundary. Consequently, the results presented provide direct evidence that the coherent twins grain boundaries (straight grain boundaries in Fig. 4) are resistant against corrosion while non coherent or random grain boundaries (curved grain boundaries in Fig. 4) are more susceptible to intergranular corrosion.

4. Conclusions

The grain-dependent electrochemical behavior of polycrystalline copper and the different intergranular corrosion performance of different grain boundaries was confirmed by using several local electrochemical techniques [1-3]. The results presented confirm the influence of the crystallographic orientation on the active dissolution of copper, these conclusions are drawn from both *ex situ* AFM measurements and *in situ* SECM experiments in combination with EBSD imaging. It was observed that under certain circumstances, not only the grain orientation has an influence on the corrosion behavior but also the orientation of the neighboring grains seems to play a decisive role in the dissolution rate. This corrosion differences are likely attributed to the different anodic/cathodic nature of the differently oriented grains and to the coupling effect when they appear together in the microstructure.

Previously reported differences of the thickness and morphology of the passive layer formed on Cu (100) and Cu (111) monocrystals in NaOH were confirmed, by means of SECM, to have a direct influence on the insulating properties.

For the first time to our knowledge, the EC-STM was used to visualize the differences in intergranular corrosion at different grain boundaries. This technique allows mapping the copper surface in a very precise manner and in this way changes on the surface at the sub-micrometer scale can be clearly visualized. While copper dissolution is clearly detected at random high angle grain boundary or at non-coherent twin boundaries, coherent twins are proved to be highly corrosion resistant.

References

1. L. Lapeire, E. Martinez Lombardia, K. Verbeken, I. De Graeve, L. Kestens, and H. Terryn, *Corros. Sci.*, **67**, 179 (2012).
2. E. M. -Lombardia, Y. G. -Garcia, L. Lapeire, I. De Graeve, K. Verbeken, L. Kestens, J. Mol, and H. Terryn, , *Electrochim. Acta*, **116**, 89 (2014).
3. E. M.-Lombardia, L. Lapeire, V. Maurice, I. D. Graeve,

K. Verbeken, L. Klein, L. Kestens, P. Marcus, and H. Terryn, *Electrochem. Commun.*, 41, 1 (2014).
4. A. Alfantazi, T. Ahmed, and D. Tromans, *Mater. Design*, **30**, 2425 (2009).
5. H.-B. Lu, Y. Li, and F.-H.Wang, *Electrochim.* Acta, **52**, 474 (2006).
6. E. Ghali, W. Dietzel, and K.-U. Kainer, *J.Mater. Eng. Perform.*, **13**, 7 (2004).
7. C. Van den Bos, H. Schnitger, X. Zhang, A. Hovestad, H. Terryn, and J. De Wit, *Corros. Sci.*, **48**, 1483 (2006).
8. F. Andreatta, H. Terryn, and J. de Wit, *Corros. Sci.*, **45**, 1733 (2003).
9. C. Caicedo-Martinez, E. Koroleva, G. Thompson, P. Skeldon, K. Shimizu, G. Hoellrigl, C. Campbell, and E. McAlpine, *Corros. Sci.*, **44**, 2611 (2002).
10. C. Yao, Z. Wang, S. L. Tay, T. Zhu, and W. Gao, *J. Alloy. Compd.*, **602**, 101 (2014).
11. A. Amirudin and S. Chawla, *J. Natl. Sci. Found.* Sri, **6**, 27 (1978).
12. V. Maurice, L. Klein, H.-H. Strehblow, and P. Marcus, *J. Phys. Chem.* C, **111**, 16351 (2007).
13. A. Seyeux, V. Maurice, L. Klein, and P. Marcus, *J. Solid State Electr.*, **9**, 337 (2005).
14. J. Kunze, V. Maurice, L. H. Klein, H.-H. Strehblow, and P. Marcus, *Electrochim. Acta*, **48**, 1157 (2003).
15. M. Vogt, A. Lachenwitzer, O. Magnussen, and R. Behm, *Surf. Sci.*, **399**, 49 (1998).
16. G. Zhou and J. C. Yang, *Appl. Surf. Sci.*, **222**, 357 (2004).
17. F. Wiame, V. Maurice, and P. Marcus, *Surf. Sci.*, **601**, 1193 (2007).
18. M. Schweinsberg, A. Michaelis, and J. Schultze, *Electrochim. Acta*, **42**, 3303 (1997).
19. B. Davepon, J. Schultze, U. König, and C. Rosenkranz, *Surf. Coat. Technol.*, **169**, 85 (2003).
20. J. R. Davis, *Copper and copper alloys*, p. ?, ASM international, Materials Park, OH (2001).
21. S. Kudelka, A. Michaelis, and J. Schultze, *Electrochim.* Acta, **41**, 863 (1996).
22. S. Kudelka and J. Schultze, *Electrochim. Acta*, **42**, 2817 (18).
23. Y. Huang and P. Prangnell, *Acta Mater.*, **56**, 1619 (7) (2008).
24. T. Konkova, S. Mironov, A. Korznikov, and S. Semiatin, *Acta Mater.*, **58**, 5262 (16) (2010).
25. T. P. Mo_at, H. Yang, F.-R. F. Fan, and A. J. Bard, *J. Electrochem. Soc.*, **139**, 3158 (11) (1992).
26. Z. Guoding, X. Qunjie, B. Loo, and A. *T. Nonferr. Metal. Soc.*, **8**, 308 (1998).
27. T. P. Moat, H. Yang, F.-R. F. Fan, and A. J. Bard, *J. Electrochem. Soc.*, **139**, 3158 (1992).
28. J. Kunze, V. Maurice, L. H. Klein, H.-H. Strehblow, and P. Marcus, *Corros. Sci.*, **46**, 245 (2004).
29. S. Kim, U. Erb, K. Aust, and G. Palumbo, *Scr. Mater.*, **44**, 835 (2001).
30. V. Randle, *Scr. Mater.*, **54**, 1011 (2006).
31. V. Gertsman and S. M. Bruemmer, *Acta Mater.*, **49**, 1589 (2001).
32. M. Kumar, A. J. Schwartz, and W. E. King, *Acta Mater.*, **50**, 2599 (2002).